Condensation on (002) graphite of liquid bismuth far below its bulk melting point

M. K. Zayed and H. E. Elsayed-Ali*
Physical Electronics Research Institute, Department of Electrical and Computer Engineering, Old Dominion University, Norfolk, Virginia 23529, USA

(Received 26 May 2005; revised manuscript received 14 September 2005; published 16 November 2005)

Condensation of thermally evaporated Bi on (002) graphite, at temperatures of 300–523 K, was studied using *in situ* reflection high-energy electron diffraction (RHEED) and room temperature *ex situ* atomic force microscopy (AFM). For deposition at temperatures below 415±5 K, transmission RHEED patterns of Bi appeared at an average thickness of ~0.5 monolayer (ML). AFM images showed that the film consisted of crystallites in the shape of triangular step pyramids with step heights corresponding to single and double Bi layers in the [111] direction. This morphology indicates crystallization from the vapor. For deposition at higher temperatures, diffuse RHEED patterns appeared independent of the deposited thickness. When these films were cooled, clear transmission patterns of crystalline Bi appeared. After cooling to near room temperature, the melting and solidification behaviors of these films were investigated with RHEED. Upon subsequent heating, the topmost layers of the probed Bi crystallites started to lose long-range order at ~10–15 K below the Bi bulk melting point, T_0=544.52 K. When crystallized from the melt, supercooling by ~125 K below T_0 was observed. These results indicate that Bi condensed on graphite in the form of supercooled liquid droplets when the graphite temperature was above 419 K (T_0–125). Below that temperature, Bi condensed in the solid phase. Bi films crystallized by cooling the liquid had crystal morphologies that depended on the degree of liquid supercooling.

DOI: 10.1103/PhysRevB.72.205426 PACS number(s): 68.03.Fg, 61.14.Hg, 68.55.Jk, 65.80.+n

I. INTRODUCTION

The nature of phase transitions and that of phases formed upon vapor condensation remain of much interest.[1,2] The presence of energy barriers for phase transitions results in asymmetry along the phase coexisting lines. For example, large supercooling of the liquid phase is readily observed, while superheating of the solid phase is not typically observed.[3–5] The phase transition mechanism remains a subject of interest, in spite of many sophisticated computer simulations and experimental studies with various probing techniques.[6–9] For crystals on the nanometer scale, reduced-size effects have introduced additional complexity to the condensation and phase transition phenomena such that the conventional pressure-temperature (*P-T*) phase diagrams become insufficient to determine the phase state of the system.[4,9–11] Because of the high surface-to-volume ratio, surface and interfacial energies play a significant role in determining the phase formation upon condensation and the properties of phase transitions. While the reduced size is known to shift the coexistence lines toward lower values, substrate or wall interactions could drive the transition temperature between the phases upward or downward based on its type.[4,9,12–15]

The subject of vapor condensation has a direct impact on many fields including crystal growth,[1] electronic device fabrication,[1,2] catalysis,[16] weather forecasting,[17] and many surface phenomena, such as wetting transition and surface reconstruction.[8,18,19] Depending on the temperature and pressure, vapor can be condensed on a substrate as a liquid or a solid. A liquid is the stable condensed phase above the bulk melting point, T_0, while a solid can be directly formed at temperatures below T_0. However, formation of the liquid phase below T_0 can also occur either due to surface melting,[19] capillary or porous condensation,[12] or eutectic alloying.[20] Moreover, suppressing heterogeneous nucleation either by small droplet size,[21,22] containerless solidification,[23] or solidification in a flux[24] can lead to the formation of metastable liquids that are deeply supercooled below T_0.

Because of its structural and thermodynamical properties, Bi has a number of phases at elevated pressures and temperatures and a wide solid-liquid hysteresis curve.[25–27] Bi in reduced dimensions has also shown many interesting physical properties that include lattice shrinking,[28,29] the presence of a metallic-semiconductor transition,[30] amorphous and metastable phase formation,[31] thermoelectricity,[32] superconductivity,[33] quantum-size effects,[34] and enhanced magnetoresistance.[35] Films deposited at liquid helium temperatures had an amorphous structure exhibiting superconductive properties,[30,33] while those deposited at 300 K up to T_0, showed a typical rhombohedral Bi structure with morphologies that vary from single crystal films to a dendrite structure.[36–43]

In general, deposition at elevated substrate temperatures increases the surface diffusion of Bi adatoms, thus producing an ordered crystalline surface; while low temperature deposition results in microscopically rough surfaces.[36–38] Bi films deposited on the [111]-BaF_2 substrate at 533 K using molecular beam epitaxy (MBE) showed a featureless scanning electron microscope (SEM) image consistent with epitaxial film formation.[39] On the other hand, films deposited at room temperature showed randomly oriented ~1 μm crystallites.[39] Bi films prepared by pulsed laser deposition (PLD) also showed a dramatic morphology dependence on the temperature of the substrate during deposition.[40] For epitaxial growth of thermally evaporated Bi on cleaved mica, preheating the substrate to 413 K and maintaining it at that

temperature during deposition was found to be essential for epitaxy.[41] This temperature was found to optimize the nucleation rate and the lateral spreading rate of Bi adatoms. Also, it was found that the Bi film is hard to nucleate on a 111-BaF_2 substrate using MBE at temperatures higher than 423 K.[42] A two-step growth process with the film initially nucleated at 373 K followed by growth to a thicker film near T_0 was employed to obtain an epitaxial film with a low level of defects and high electron mobility.

Reflection high-energy electron diffraction (RHEED) is a structurally sensitive probe used to obtain real-time information on the top monolayers of a surface, either during film growth or a surface phase transition.[44,45] In the present work, *in situ* RHEED is used to monitor the deposition of Bi on a highly oriented (002) graphite surface. *Ex situ* atomic force microscopy (AFM) is used to study the morphology of the deposited films. Two deposition regimes were observed; growth of solid crystallites below a substrate temperature of 413 ± 5 K, and condensation of the liquid phase above that temperature. The melting point size dependence of the initially formed nuclei, combined with the thermal characteristics of Bi is used to explain liquid Bi formation below T_0 on the graphite surface. The morphology of films crystallized from the condensed liquid Bi, was found to be different from those directly crystallized from the vapor. The dependence of the formed morphology on the degree of liquid supercooling is also discussed.

II. EXPERIMENTAL METHOD

The experiment was performed in an ultrahigh vacuum (UHV) chamber with a base pressure in the mid 10^{-10} Torr. Highly oriented pyrolytic (002) graphite (HOPG) was used as a substrate. HOPG is chemically inert. Accordingly, the deposited Bi interacts with the graphite substrate via the van der Waal attraction force with no interdiffusion or chemical compound formation.[43] The graphite substrate is loaded in the UHV chamber immediately after cleaving it in air. The substrate is mounted on a resistively heated stage capable of reaching temperatures up to 1000 K. A RHEED system is available in the UHV chamber and is used to monitor the substrate. The graphite substrate is heated to ~770 K for 10 min in order to evaporate any adsorbed gases and obtain a clear graphite RHEED pattern. By controlling the current passing through the heating stage, the substrate temperature can be varied. A *K* type thermocouple placed in contact with the substrate surface is used to measure the temperature. The thermocouple is calibrated in air to the bulk melting point of pure Bi. This calibration is performed before and after the experiment in order to assure that the properties of the thermocouple were not altered during the heating and cooling cycles. A temperature measurement uncertainty of ±1 K was obtained.

Bi with 99.999% purity is evaporated from a resistively heated tungsten basket. The film mean thickness is obtained using a calibrated quartz crystal thickness monitor. By controlling the current applied to the heater filament, the deposition rate is maintained between 0.4–0.7 Å s^{-1}. Bi has an average Bi-Bi bond length of 3.24 Å, which is used to express the measured film thickness in ML.

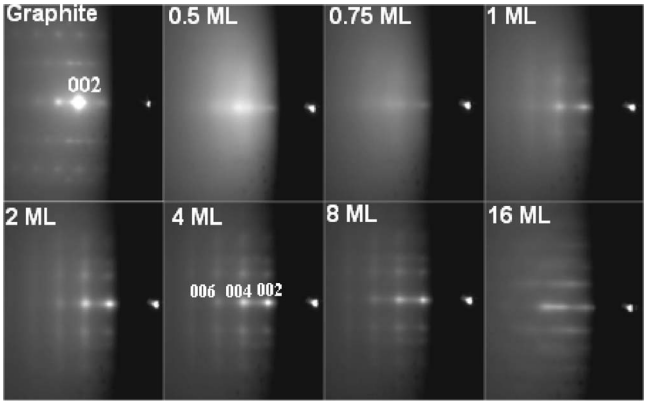

FIG. 1. Real time RHEED patterns taken during Bi deposition at room temperature. The graphite spot intensity decays and that of Bi start to appear after a deposition of ~0.5 ML. The spot intensities of Bi increase with the deposited thickness up to ~8 ML. Elongated RHEED streaks at 16 ML indicate coalescence and formation of asymmetric shape crystallites.

RHEED diffraction patterns are obtained using a 9.7 kV electron beam. A computer-controlled charged coupled device (CCD) camera is used to record the diffraction patterns that are displayed on a phosphorus screen. Real time RHEED patterns are obtained during film deposition to study the structural evolution of Bi deposited at different temperatures. Each RHEED pattern is acquired in about 170 to 400 ms, depending on the image quality. After film completion, the chamber is vented to atmospheric pressure using argon gas and the films are taken out for surface morphology studies. An *ex situ* AFM operated in the tapping mode with lateral and height resolutions of 1 nm and <0.1 nm, respectively (as specified by the manufacturer) is used. Films deposited at different deposition temperatures were studied.

III. RESULTS AND DISCUSSION

A. Low temperature solid film deposition

After heating and then cooling the graphite substrate, the RHEED pattern, taken at room temperature, indicated a transmissionlike diffraction pattern consisting of spots aligned along rods normal to the surface. The RHEED pattern of the graphite surface was indexed based on three-dimensional (3D) reciprocal lattice spots seen in the $1\bar{1}0$ zone with the electron beam parallel to the zone axis. Detailed analysis of the graphite RHEED pattern can be found elsewhere.[46] The diffraction features observed were consistent with a clean graphite surface. Thermal deposition of Bi on graphite was studied by obtaining real time RHEED images during deposition. Figure 1 shows RHEED patterns of the surface with different Bi coverages deposited at room temperature. The graphite spot intensity becomes dim at a Bi coverage of 0.5 ML and a diffuse background appears. As the deposited film thickness is increased to an average of 4–6 ML, the diffraction intensities of the Bi spots increase. Indexing of these spots show that they are characteristic of the rhombohedral structure of Bi. The RHEED intensity of the

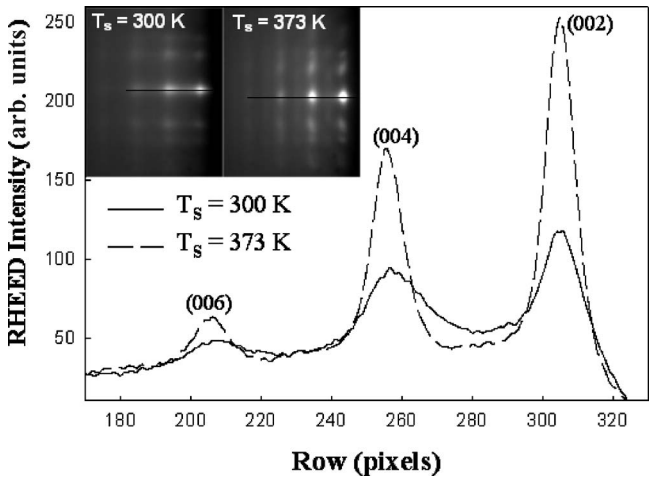

FIG. 2. Line profiles, normal to the substrate surface, of RHEED patterns taken after deposition of 8 ML Bi films deposited at two different substrate temperatures (T_s).

(002) graphite spot decayed continuously with Bi deposition and showed no intensity oscillation. This behavior is consistent with 3D growth forming islands. The intensity of the (002) Bi spot increased with the deposited thickness. After deposition of ~8 ML, the Bi diffraction spot intensity monotonically decreased. The increase of the Bi diffraction intensity and reduction of the graphite diffraction intensity is due to the increase in the surface coverage with Bi. However, as the Bi coverage was further increased, the density of misaligned crystallites increased resulting in a decrease in the Bi RHEED spot intensity. After deposition of ~16 ML, the shape of the Bi spots changed from nearly rounded to elongated streaks, with the major axis normal to the substrate surface. Elongated RHEED spots indicate the formation of crystals with asymmetric shape, which was confirmed later using *ex situ* AFM. With further Bi deposition, the elongated RHEED spots remained almost the same with no shape change. Films deposited at a substrate temperature of 373 K showed RHEED patterns that were thickness dependent similar to that observed for those deposited at room temperature but with no noticeable elongation in the spots at higher thicknesses.

For Bi films deposited on graphite with the substrate temperature between 300 K and 373 K, no change in the relative spot positions was observed with the deposited thickness. This remained the case from the initial formation of detectable transmission Bi spots up to the maximum studied Bi thickness. Also, no change in the relative spot position was observed as the deposition temperature was increased from 300 to 373 K, indicating no change in the film growth direction. Figure 2 shows line profiles of Bi RHEED patterns in a direction normal to the substrate surface for 8 ML films deposited at 300 and 373 K. Narrower peaks with higher intensities were observed for films deposited at 373 K. This indicated that films deposited at 373 K have an enhanced average crystallite size and/or a higher degree of orientation relative to those deposited at room temperature.

Ex situ AFM in air was used to study the structural morphology of the films after deposition. Figure 3 shows the obtained images for 25 ML Bi films deposited at 300 and 373 K along with the corresponding RHEED patterns obtained in the deposition chamber, after terminating the deposition. The AFM images show highly ordered, 3D crystallites with layered triangular pyramidlike shapes. The edges of these crystallites become more defined and sharper as the deposition temperature is increased. The morphology of the formed crystallites indicates that Bi adatom nucleation on the top of a triangular Bi layer is likely. The growth of these nuclei occurs simultaneously with the lateral growth of the layer underneath in a 2D layer-by-layer-like growth mode. This crystal shape and growth mode results in elongated RHEED spots that continuously decay in intensity with deposition. This is because the average lateral crystalline size parallel and normal to the electron path are not equal due to the triangular pyramid surface morphology. RHEED intensity is sensitive to growth dynamics within the electron penetration depth over the probed area. Since the growth occurs concurrently in isolated crystallites with different heights, no RHEED intensity oscillation of the (002) Bi spot was observed, in spite of the layer-by-layer growth in each pyramid. Similar triangular-shaped crystallites formed by the same growth mode were previously reported for epitaxial Bi films deposited on a cleaved mica substrate.[41,47] This growth mode indicates solid film formation from the vapor phase. The ob-

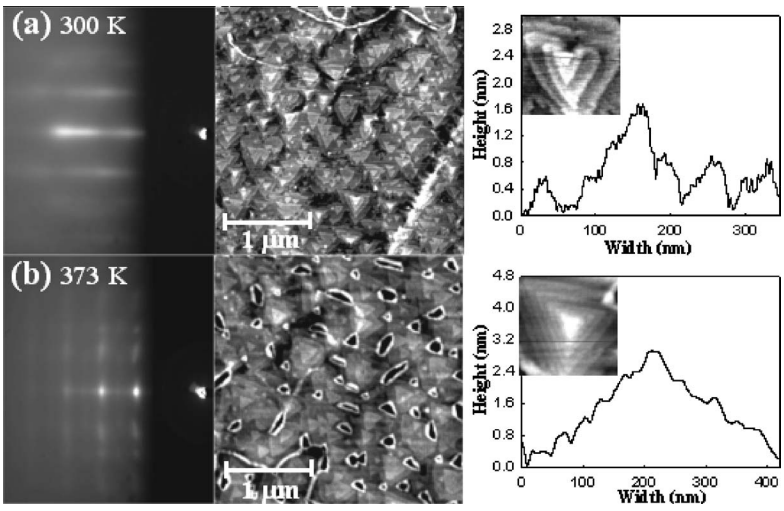

FIG. 3. RHEED pattern and *ex situ* AFM images along with line profiles of AFM through a smaller scanned area of 25 ML Bi films deposited at two different substrate temperatures: (a) T_s = 300 K and (b) T_s = 373 K.

served orientational epitaxy can occur when the adsorbate has a weak interaction with the substrate. In this case the overlayer has a lattice spacing different from that of the substrate but grows with an orientation that is affected by the substrate.[48,49] For a graphite substrate, Bi adatoms were reported to be highly mobile on its basal plane and the growth was site limited rather than diffusion limited.[50] Thus, the epitaxial layer of Bi was observed to grow in directions of minimum lattice and angular mismatch with the graphite substrate.

As the substrate temperature was increased from 300 to 373 K, the number of triangular crystallites found in the scanned area decreased. While this observation suggests a decrease in the nucleation density with temperature, other possible causes include ripening, annealing due to deposition at a higher temperature, and coalescence are also possible. From Fig. 3, an enhancement in the lateral growth of the deposited Bi and increased coalescence during growth is observed for films deposited at 373 K as compared to films deposited at 300 K. This enhancement in lateral size and the decrease in the crystallite density results in the transformation of wide elongated RHEED spots shown in Fig. 3(a) to the small circular spots shown in Fig. 3(b). The full width at half maximum of the RHEED spots is reduced with increased crystal size. Increased coalescence at 373 K leads to trench formation forming voids in the Bi film due to coalescence of misorientated neighboring islands. The step heights forming the triangular pyramid structure in Figs. 3(a) and 3(b) were mostly found to be 0.4 ± 0.1 nm, while a small number were 0.8 ± 0.1 nm. The Bi structure can be visualized as a layered hexagonal structure in the [111] direction with $d_{111}=11.862$ Å, containing three successive layers with a 3.9 Å separation distance. Thus, the measured step heights correspond to single and double heights of the Bi structure with its (111) facet oriented parallel to the substrate surface in pseudocubic notation. Measurements of the terrace heights showed no variation with deposition temperatures within the studied range.

B. High temperature liquid phase condensation

RHEED observation of Bi deposition at different graphite substrate temperatures showed that solid crystalline films were directly formed on the surface for substrate temperatures up to ~410 K. The lowest substrate temperature considered was 300 K. As the graphite substrate temperature was increased higher than 373 K, the Bi diffraction pattern became weaker when compared to films of equal thickness deposited at different temperatures. Figure 4(a) shows RHEED patterns taken during deposition of a 25 ML Bi film deposited at substrate temperatures ranging from 403 to 418 K. The reduction in the RHEED spot intensity with substrate temperature can be seen by comparing Fig. 4(a) with that of Fig. 3(b) taken at 373 K. The intensity of the (002) spot of the 25 ML film deposited at 410 K remained almost constant for a period of hours after deposition. However, a faint diffraction pattern that slowly increased in intensity after deposition of 25 ML was observed for films deposited and maintained at 413 K. Films deposited

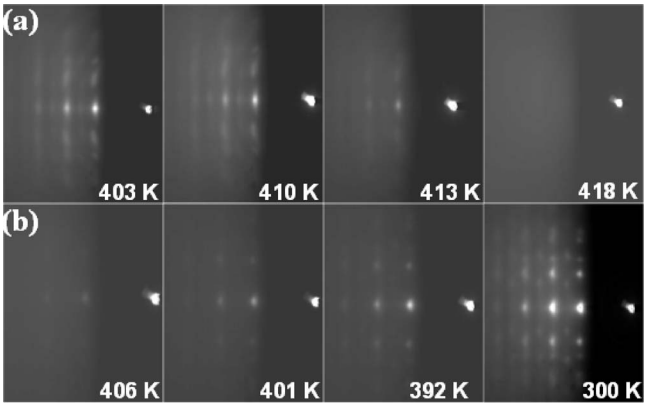

FIG. 4. (a) RHEED pattern taken after deposition of 25 ML Bi films at different substrate temperatures. The deposition temperature of $\sim 415\pm5$ K is the solid-liquid formation boundary. (b) RHEED pattern taking during cooling to room temperature of 25 ML Bi film initially deposited at 433 K.

at temperatures higher than or equal to 418 K showed a diffuse pattern with a background intensity that decreased with increased film thickness. This diffuse pattern remained unaffected by the deposited Bi thickness up to 100 ML. Also, when a 25 ML film was left overnight at the 418 K deposition temperature, no change in the RHEED intensity was observed. However, when these films were cooled, a transmission RHEED pattern started to appear in the temperature range between 406 and 392 K as shown in Fig. 4(b). Strong RHEED patterns corresponding to twinned or multiazimuth orientations were observed as the temperature was decreased to 300 K. A diffuse diffraction pattern is an indication of the lack of long-range order in the deposited film. The appearance of a Bi diffraction pattern after cooling below the supercooling limit indicates that these Bi films were initially formed in the liquid phase and precludes the possibility that a solid amorphous film was initially formed.

Condensation of liquid films on different substrates at temperatures less than their bulk melting points was previously reported. In a pulsed laser deposition experiment of Bi on a glass substrate, followed by the observation of film morphology using *ex situ* scanning tunnel microscope and AFM, it was concluded that the film condensed in the liquid phase when deposition was performed with the substrate temperature at 458 K. The liquid droplets crystallized with cooling forming submicron spherical shaped isolated crystallites.[51] At lower deposition temperatures, Bi nucleated directly into the solid phase forming films with smooth surfaces.[51] Deposition of Bi on Si(100) did not show similar behavior. Thus, formation of the liquid phase in pulsed laser deposition was attributed to the high energy of the laser-ablated Bi and the absence of substrate influence. Scanning tunneling microscopy, Auger electron spectroscopy, and x-ray photoelectron spectroscopy revealed the formation of indium nanodrops in a 6 ML thermally deposited film on a Ge(001) substrate in UHV at room temperature.[52] The presence of indium in the liquid phase, even at room temperature, was attributed to the internal stress resulting from the lattice mismatch between the film and the substrate, and to the reduced dimensionality of the deposited film. Both fac-

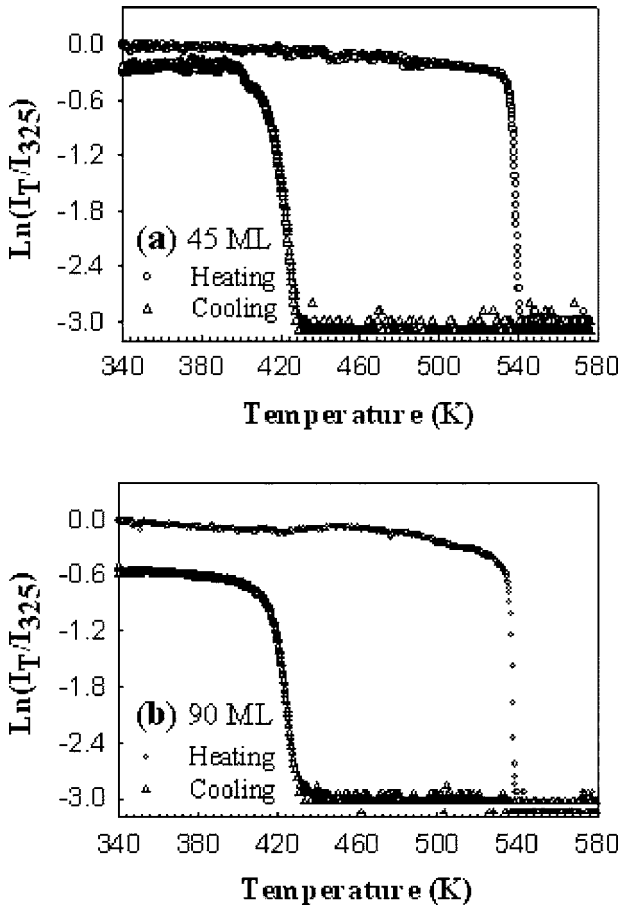

FIG. 5. Natural logarithm of the normalized RHEED intensity of the (002) Bi spot as a function of temperature during heating and cooling of (a) 45 ML and (b) 90 ML Bi films initially deposited at 423 K.

tors are known to decrease the equilibrium melting point. Also, liquid Bi droplets with spherical shapes were previously detected using *in situ* electron microscopy for films deposited at temperatures above 423 K and having dimensions less than 150 Å.[53] Coalescence as well as transformation of these droplets into solid crystals during growth were observed.

RHEED probes a layer of an average thickness given by the inelastic mean free path which is ~9 nm for the 9.7 kV RHEED electron beam.[54] Thus, diffuse RHEED patterns could be due to surface melting or due to liquid phase condensation. In order to differentiate between these two possibilities, the film was cooled to 300 K then the RHEED intensity of the (002) Bi spot was measured as a function of temperature. The intensity was normalized to that measured at 325 K. Figure 5 shows the natural logarithm of the normalized RHEED intensity of the (002) spot for 45 ML and 90 ML Bi films deposited at 423 K. A decrease in the spot intensity with temperature was expected due to the enhanced atomic mean vibrational amplitude as described by the Debye-Waller effect.[54] However, a sharp drop in the RHEED intensity occurred as the nanocrystals lose long-range order within the shell probed by the electron beam, which appeared only at ~10–15 K below the bulk melting point of bismuth, T_0=544.52 K. The normalized intensity vanished at ~4 K below T_0, indicating complete film melting. During cooling, the liquid Bi remained in the liquid phase down to 418 K, ~125 K below T_0. This behavior was reproducible after the first heating-cooling cycle with an ~4–10 K shift toward higher temperatures for the onset of melting and freezing. Within the experimental error, no significant change in the RHEED pattern behavior was observed with further heating and cooling. Films deposited at room temperature also showed reproducible heating-cooling hysteresis curves; however, in this case with a small shift towards lower temperatures for the onset of melting and freezing. These observed shifts are expected to be due to the dependence of the solid-liquid transition on the size distribution and/or shape of the crystallites, which changes with heating and melting after deposition. Surface melting is a reversible phase transition with a defined onset point for clean surfaces.[24] Since the decrease in the measured RHEED intensity due to surface melting occurred only within a few degrees from T_0, we conclude that Bi condensed as liquid droplets at temperatures as low as 125 K below T_0.

Condensation of liquid Bi at a substrate temperature as low as T_0-125 K cannot be simply explained based on substrate effect since graphite is an inert substrate with no known chemical reactivity with Bi and, therefore, should have only a weak influence on growth that is limited to orientational epitaxy described earlier. The condensation of liquid Bi from the vapor is most likely related to the tendency of Bi to show a large degree of supercooling and size dependent melting point depression. It is interesting that the T_0-125 maximum supercooling temperature that we observed for Bi in Fig. 5 was the same as the lowest temperature for which condensation of liquid Bi from the vapor occurred. Melting point depression by few degrees was observed in Fig. 5, but is known to be strongly dependent on size for Bi nanocrystals as well as other nanocrystals.[13,29]

The size effect on the melting point was described by different phenomenological models.[29,55,56] All of them predict a melting point depression proportional to the reciprocal of the particle radius. Examples of these models are the homogenous melting model,[13,55] the liquid drop model,[56] and the lattice vibration-based model.[29] In the homogenous melting model, the melting point is the point at which the melt and the solid coexist homogenously in equilibrium. According to this model, the size dependence of the melting point is described by[13,55]

$$T_m = T_0 - \frac{2T_0}{\rho_s L r}\left[\gamma_s - \gamma_l\left(\frac{\rho_s}{\rho_l}\right)^{2/3}\right], \quad (1)$$

where T_0 is the bulk melting point, T_m is the melting point of a particle of radius r, L is the latent heat of fusion, and γ_s, γ_l and ρ_s, ρ_l are the surface energy per unit area and the density of the solid and liquid phases. In the liquid drop model, empirical relations among the cohesive energy, surface tension, and melting temperature are used, in an analogy to the liquid-drop model used in describing the nucleus structure. An expression for the size-dependent melting for low-dimensional systems is derived such that[56]

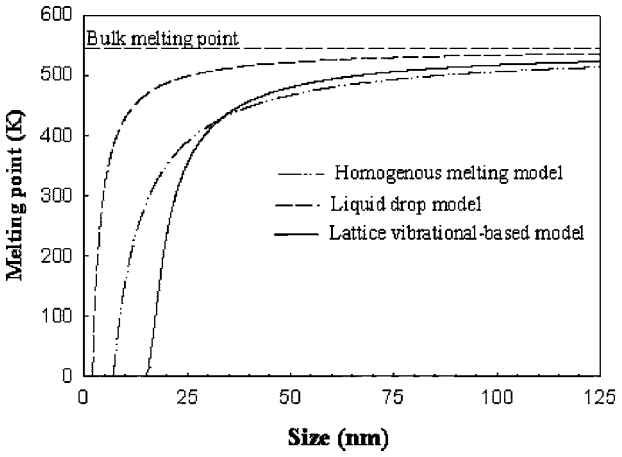

FIG. 6. Melting point size dependence of Bi as calculated from different models.

$$T_m = T_0\left(1 - \frac{\beta}{r}\right), \tag{2}$$

where β is a surface energy dependent constant given for Bi to be equal to 2.1273 nm.[55] Another approach that does not include any adjustable parameter is based on Lindemann's criterion and Mott's expression of the vibrational entropy, which give a melting point–size-dependent formula as[29]

$$T_m = T_0 \exp\left(\frac{-(2S_{\mathrm{vib}}/3R)}{\frac{r}{6h} - 1}\right), \tag{3}$$

where S_{vib} is the vibration entropy of melting of the bulk crystal, h is the atomic diameter, and R is the ideal gas constant. The known physical constants of Bi (T_0=544.52 K, ρ_s=9.8 g/cm^3, ρ_l=10.07 g/cm^3, $L=5.19\times10^{-8}$ erg/g, γ_{sl} =61 erg/cm^2, γ_{sv}=550 erg/cm^2, γ_{lv}=375 erg/cm^2, h =0.4074 nm, S_{vib}=3.78 J mole^{-1} K^{-1}, and R =8.3142 J mole^{-1} K^{-1}) are used to calculate the melting point size dependence of Bi.[29,55,56] Figure 6 shows the size-dependent behavior predicted by these models. Although these models show the same trend, there is some discrepancy at smaller sizes. Also, these models consider only spherical-shaped particles and do not include the crystallite shape effect. Therefore, the predicted melting point of the particle is only an estimate. From Fig. 6, particles with sizes between 5–20 nm can melt at room temperature. At 420 K, both the homogenous melting model and the lattice vibrational-based model predict that a particle of ~32 nm size would melt, while the liquid drop model requires that the particle size be less than ~8 nm to melt at 420 K. Considering the 0.203 nm atomic radius of the Bi atom, these sizes correspond to clusters containing roughly 4×10^6 atoms for the 32 nm cluster and 6×10^4 atoms for the 8 nm cluster, which are apparently very large compared to that necessary to form stable nuclei. Based on the above, one would suggest that the Bi nuclei are originally formed in the liquid phase because of the size-dependent melting point depression. However, as the nuclei grew, they solidified when the deposition temperature was below the freezing point. This freezing point is observed from Fig. 5 to be between 410 and 424 K based on a RHEED measurement of films solidified from the melt. From the RHEED observation of Bi condensed on graphite, we observed a pattern for temperatures below 415±5 K (Fig. 4), which is in agreement with the maximum supercooling temperature, obtained from Fig. 5, within the expected experimental error. Thus, the liquid nuclei grew and remained in the liquid phase when the films were deposited at temperatures above the maximum possible supercooling temperature.

For a deposition substrate temperature above the maximum supercooling point, the liquid Bi nuclei will be trapped in the supercooling state and grow forming larger size liquid droplets. The small size of the stable nucleus in the Bi-graphite system, relative to crystallites obtained at growth termination, reduces the melting point of the stable nucleus and increases the amount of supercooling, as predicted by different size-dependent melting models and observed experimentally.[21,22,29,55,56] The values of surface, interfacial, and bulk free energies involved in nanocrystal growth affect the size of the stable nucleus. In general, the amount of supercooling is affected by the size of the crystal as well as the melting and freezing kinetics.[22,57,58] For clusters of sizes larger than the stable nucleus, the amount of supercooling was reported to vary linearly with the reciprocal of the cluster size, assuming heterogeneous solidification due to its dominance and low activation energy.[57] In Fig. 5, we observed an amount of supercooling for 45 ML that is ~4 K larger than that for 90 ML, which is attributed to the average size increase with the film coverage.

In order to study the effect of the freezing kinetics on the film supercooling, we obtained melting-freezing curves similar to those of Fig. 5, but with different cooling rates. The films were cooled from the same initial liquid overheating point, 10 K above T_0 of Bi. As the cooling rate was increased from 0.9 K/min to 9.5 K/min, an ~6 K increase in the film maximum supercooling was observed. These cooling rates are the experimentally feasible rates using the current setup. The effect of the cooling rate on the amount of melt supercooling was reported to vary. For slow cooling rates, the amount of supercooling remains basically unchanged. For example, for PbTe no dependence on the cooling rate was observed for cooling rates between 0.5 and 3.0 K/min.[58] With the increase in the cooling rate the amount of supercooling could increase. For example, the amount of supercooling changed by ~46 K as the cooling rate was increased from 90 to 456 K/min for $Bi_{95}Sb_5$.[59] The ~6 K shift that we observed in the amount of supercooling with the cooling rate is about the same as the stated error in the RHEED observation of the solid/liquid formation boundary for Bi condensation on graphite, 415±5 K. In addition, to check on the stability of supercooled Bi droplets, melted Bi crystallites were left in the supercooled state overnight at 10–15 K above the freezing edge. No sign of solidification was observed, indicating that Bi has a stable supercooled liquid. Thus, within the studied experimental conditions, the freezing rate has little effect on the kinetics of liquid condensation due to the relatively large and stable supercooling of Bi nanodroplets.

The AFM analysis of films crystallized from the melt showed that these films have morphologies different from those grown from the vapor. While triangular layered shape

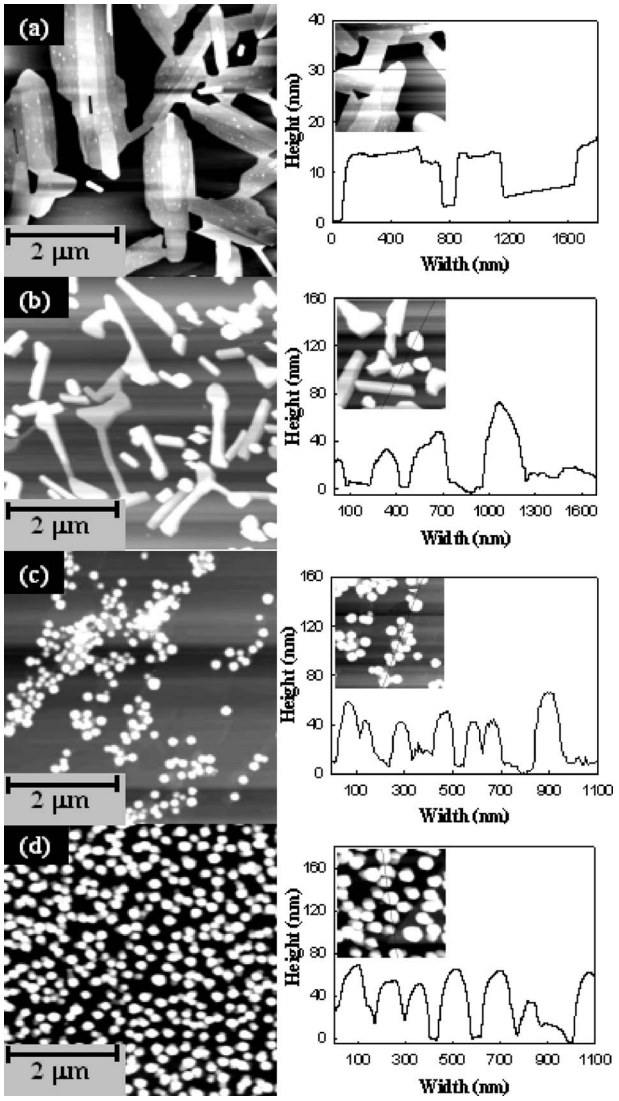

FIG. 7. AFM images, along with line profiles of Bi films deposited at different temperatures: (a) 25 ML deposited at 413 K, (b) 25 ML deposited at 423 K, (c) 25 ML deposited at 453 K, and (d) ~33 ML deposited at 498 K.

crystallites were formed at a substrate temperature of 300–373 K, rounded or elongated platelet shaped crystallites were formed for films deposited at 413–598 K. Figure 7 shows some *ex situ* AFM images and line profiles of films deposited at substrate temperatures between 413 and 532 K. Two different morphologies could be recognized based on the film deposition temperature. Those deposited in the neighborhood of the solid/liquid condensation temperature, which is the maximum supercooling point 415±5 K, form elongated platelet shaped crystals, while those deposited at higher temperatures form rounded polyhedral crystals. Films deposited at 413 K, a few degrees below the maximum supercooling point, showed relatively wide elongated crystallites with almost flat top surfaces. These films produced a faint RHEED pattern, as shown in Fig. 4(a). Films deposited at 423 K, several degrees above the maximum supercooling temperature, had crystallites of mixed shapes consisting of rodlike and rounded crystallites with curved top surfaces. These films produced diffuse RHEED patterns similar to those deposited at 418 K, as shown in Fig. 4(a). Finally, films deposited at a substrate temperature of 453 and 498 K showed almost identical rounded polyhedral crystallites with curved top surfaces. Furthermore, the triangular shape Bi crystallites formed in films deposited at temperatures 300 and 373 K changed into a rounded polyhedral shape similar to that of Figs. 7(c) and 7(d) after heating by a few degrees above T_0 and then cooling to room temperature. Because the RHEED image is due to diffraction from crystallites forming the film within the probed area and is affected by shadowing, no significant change in the diffraction pattern after cooling to 300 K was observed for films crystallized from the liquid phase. Misalignment or randomness of the film crystallites in addition to height differences between the crystallites, shown in Fig. 7, increased the shadowing effect and the shape and size insensitivity of RHEED.[60]

The different crystallographic shapes of crystallites deposited at temperatures near 415±5 K or higher then cooled to room temperature indicate that the morphology is affected by the degree of liquid supercooling of the initially condensated liquid. Because of the presence of an energy barrier for solid nucleation, which is affected by the volume change upon solidification and the release of latent heat, the melt can be supercooled. The presence of short-range order is characteristic of a supercooled melt.[7,59,61] The melt stays in this metastable supercooled state until spontaneous homogenous or heterogeneous solidification occurs. The height of the energy barrier for solidification decreases as the amount of supercooling increases resulting in an increase in the solidification rate and/or growth velocity. Thus, different crystallographic structures may be formed depending on the initial supercooling point of the melt. Negative volume change upon melting is a shared property between Bi and water. For water, it is due to the formation of a low-density cage structure created by hydrogen bonds, which link one water molecule to the next.[21,62] For Bi, the negative volume change upon melting is thought to be due to liquid Bi having well-defined long-lived high-density clusters.[62] For ~4.5–7.5 nm liquid Bi clusters supported on weakly interacting carbon substrates, measurements of the changes in the vibrational spectra of these clusters during solid-liquid transition using interference enhanced Raman spectroscopy showed no change in the short-range order including bond distances, the number of nearest neighbors, and the bond angle-distribution disorder.[63] A neutron diffraction study showed that there is some similarity between the structure of liquid and solid Bi.[64] We also note that water crystallizes with different morphologies and structures based on the initial supercooling point from which the liquid is crystallized.[21]

Thus, we conclude that the formation of different crystallographic shapes upon cooling of the deposited Bi crystallites is due to solidification from different supercooling regions. Rodlike Bi crystallites were formed for films deposited at substrate temperatures between 413 and 423 K. At these temperatures, the condensed Bi nucleates in the form of a highly supercooled liquid that can be described as a quasiliquid with short-range order.[61] Considering that solid Bi has a highly anisotropic structure and its highly super-

cooled melt has properties closer to that of the solid than to the liquid, the formation of these crystal shapes can be explained by the presence of order in the supercooled melt. Highly anisotropic crystal growth that induces anisotropic crystal shapes has been previously reported for Bi films grown by PLD.[26] Rounded or polyhedral crystal shapes were formed for Bi films solidified from less supercooled liquids where atoms have higher mobility and less anisotropic properties.

IV. SUMMARY AND CONCLUSION

In situ real time RHEED and *ex situ* AFM were used to study the structure and morphology of Bi deposited on graphite at different temperatures. Two deposition regimes were found; low temperature solid film deposition and high temperature liquid phase condensation. A substrate temperature of 415±5 K was found to be the boundary between these two regimes.

Films deposited at temperatures below 415±5 K showed transmission RHEED patterns corresponding to the Bi structure at an average thickness as low as ~0.5 ML, indicating direct solid film formation. The continuous decay of the graphite (00) spot intensity indicated 3D Bi island formation. AFM analysis showed that these films were composed of 3D multilayer triangular step-pyramid shaped crystallites. This crystallite shape supports the conclusion of direct solid Bi crystallites growth from the vapor phase in a 2D layer-by-layer-like growth mode.

Bi deposited at temperatures higher than 415±5 K condensed into liquid droplets. This result is supported by the observation of diffuse RHEED patterns that are thickness independent. When these films were cooled, clear transmission RHEED patterns appeared in the temperature range between 408 and 392 K. Moreover, when these films were subsequently heated, the diffuse RHEED patterns appeared only at ~10–15 K below T_0 of Bi, due to surface melting forming a liquid shell surrounding the crystallite. Upon cooling, these Bi crystallites supercooled by ~125 K. Our observations indicate that not only the surface but also the bulk of the deposited Bi films were condensed in a long-lived, relatively stable, supercooled liquid phase. Different size-dependence melting point models support the conclusion that Bi is condensed in a liquid phase for substrate temperatures higher than 415±5 K. As the Bi nuclei grew in size, it solidified when it reached a certain critical size that is dependent on temperature. However, the liquid nuclei would remain in the liquid phase if the films were deposited on substrates with temperatures above the maximum supercooling point.

AFM observation of Bi crystallized from a liquid showed that two different crystal shapes are formed based on the deposition temperature. Films deposited in the neighborhood of the solid-liquid condensation temperature boundary, 415±5 K, form crystallites with nonisotropic shapes, while those deposited at higher temperatures form rounded polyhedral crystallites. The different crystallographic shapes observed for these films result from the dependence of crystal morphology on the degree of liquid supercooling.

ACKNOWLEDGMENTS

This material is based upon work supported by the U.S. Department of Energy, Division of Material Sciences, under Grant No. DE-FG02-97ER45625, and by the National Science Foundation under Grant Nos. DMR 9988669 and 0116015.

*Corresponding author. Electronic address: helsayed@odu.edu

[1] S. A. Kukushkin and A. V. Osipov, Prog. Surf. Sci. **51**, 1 (1996).
[2] P. Meakin, Rep. Prog. Phys. **55**, 157 (1992).
[3] S. N. Luo, T. J. Ahrens, T. Cagin, A. Strachan, W. A. Goddard III, and D. C. Swift, Phys. Rev. B **68**, 134206 (2003).
[4] F. Banhart, E. Hernández, and M. Terrones, Phys. Rev. Lett. **90**, 185502 (2003).
[5] S. Luo and D. C. Swift, J. Chem. Phys. **121**, 7387 (2004).
[6] S. J. Zhao, S. Q. Wang, D. Y. Cheng, and H. Q. Ye, J. Phys. Chem. B **105**, 12857 (2001).
[7] T. Schenk, D. Holland-Moritz, V. V. Simonet, R. Bellissent, and D. M. Herlach, Phys. Rev. Lett. **89**, 075507 (2002).
[8] C. Liu, S. Yamazaki, R. Hobara, I. Matsuda, and S. Hasegawa, Phys. Rev. B **71**, 041310(R) (2005).
[9] F. Calvo and F. Spiegelmann, Phys. Rev. Lett. **82**, 2270 (1999).
[10] M. Wautelet, J. P. Dauchot, and M. Hecq, Mater. Sci. Eng., C **23**, 187 (2003).
[11] N. Maeda and H. K. Christenson, Colloids Surf., A **159**, 135 (1999).
[12] H. K. Christenson, Phys. Rev. Lett. **74**, 4675 (1995).
[13] T. Castro, R. Reifenberger, E. Choi, and R. P. Andres, Phys. Rev. B **42**, 8548 (1990).
[14] L. Zhang, Z. H. Jin, L. H. Zhang, M. L. Sui, and K. Lu, Phys. Rev. Lett. **85**, 1484 (2000).
[15] H. W. Sheng, G. Ren, L. M. Peng, Z. Q. Hu, and K. Lu, Philos. Mag. Lett. **73**, 179 (1996).
[16] F. Bagnoli, B. Sente, M. Dumont, and F. L. Dagonnierb, J. Chem. Phys. **94**, 777 (1991).
[17] R. G. Harrison, Space Sci. Rev. **94**, 381 (2000).
[18] A. Esztermann, M. Heni, H. Lowen, J. Klier, M. Sohaili, and P. Leiderer, Phys. Rev. Lett. **88**, 055702 (2002).
[19] J. F. van der Veen, Surf. Sci. **433–435**, 1 (1999).
[20] M. Ikeda, T. Shibata, H. Aoki, and T. Itami, J. Non-Cryst. Solids **312–314**, 217 (2002).
[21] M. Akyurt, G. Zaki, and B. Habeebullah, Energy Convers. Manage. **43**, 1773 (2002).
[22] S. V. Dukarov, Thin Solid Films **323**, 136 (1998).
[23] P. Ayotte, R. S. Smith, G. Teeter, Z. Dohnálek, G. A. Kimmel, and B. D. Kay, Phys. Rev. Lett. **88**, 245505 (2002).
[24] Y. Shao and F. Spaepen, J. Appl. Phys. **79**, 2981 (1996).
[25] H. Lwasaki, J. H. Chen, and T. Kikegawa, Rev. Sci. Instrum. **66**, 1388 (1995).
[26] E. Haro-Poniatowski, R. Serna, C. N. Afonso, M. Jouanne, J. F. Morhange, P. Bosch, and V. H. Lara, Thin Solid Films **453–454**,

467 (2004).
[27] N. B. Thoftt, J. Bohrf, B. Burast, E. Johnsons, A. Johansens, H. H. Andersens, and L. Sarholt-Kristensens, J. Phys. D **28**, 539 (1995).
[28] X. F. Yu, X. Liu, K. Zhang, and Z. Q. Hu, J. Phys.: Condens. Matter **11**, 937 (1999).
[29] L. H. Liang, J. C. Li, and Q. Jiang, Physica B **334**, 49 (2003).
[30] M. M. Rosario and Y. Liu, Phys. Rev. B **65**, 094506 (2002).
[31] M. G. Mitch, S. J. Chase, J. Fortner, R. Q. Yu, and J. S. Lannin, Phys. Rev. Lett. **67**, 875 (1991).
[32] J. P. Heremans, C. M. Thrush, D. T. Morelli, and M.-C. Wu, Phys. Rev. Lett. **88**, 216801 (2002).
[33] T. Hamadat, K. Yamakawa, and F. E. Fujita, J. Phys. F: Met. Phys. **11**, 657 (1981).
[34] K. Liu, C. L. Chien, and P. C. Searson, Phys. Rev. B **58**, R14681 (1998).
[35] F. Y. Yang, K. Liu, K. Hong, D. H. Reich, P. C. Searson, and C. L. Chien, Science **421**, 1335 (1999).
[36] A. Martinez, R. Collazo, A. R. Berrios, and G. O. Ducoudray, J. Cryst. Growth **174**, 845 (1997).
[37] S. Jiang, Y.-H. Huang, F. Luo, N. Du, and C.-H. Yan, Inorg. Chem. Commun. **6**, 781 (2003).
[38] Y. Namba and T. Mori, J. Appl. Phys. **46**, 1159 (1974).
[39] D. L. Partin, J. Heremans, D. T. Morelli, C. M. Thrush, C. H. Olk, and T. A. Perry, Phys. Rev. B **38**, 3818 (1988).
[40] A. Dauscher, A. Jacquot, and B. Lenior, Appl. Surf. Sci. **186**, 513 (2002).
[41] J. Jing, P. N. Henriksen, H. T. Chu, and H. Wang, Appl. Surf. Sci. **62**, 105 (1992).
[42] D. L. Partin, C. M. Thruch, J. Heremans, D. T. Morelli, and C. H. Olk, J. Vac. Sci. Technol. B **7**, 348 (1989).
[43] H. Wang, J. Jing, and P. N. Henriksen, J. Vac. Sci. Technol. A **11**, 1987 (1993).
[44] Y. Shigeta and Y. Fukaya, Appl. Surf. Sci. **237**, 21 (2004).
[45] K. Theis-Bröhl, I. Zoller, P. Bödeker, T. Schmitte, H. Zabel, L. Brendel, M. Belzer, and D. E. Wolf, Phys. Rev. B **57**, 4747 (1998).
[46] Z. H. Zhang, P. Kulatunga, and H. E. Elsayed-Ali, Phys. Rev. B **56**, 4141 (1987).
[47] H. Wang, J. Jing, R. R. Mallik, H. T. Chu, and P. N. Henriksen, J. Cryst. Growth **130**, 571 (1993).
[48] A. Koma, K. Sunouchi, and T. Miyajima, J. Vac. Sci. Technol. B **3**, 724 (1985).
[49] L. W. Bruch, M. W. Cole, and E. Zaremba, *Physical Adsorption: Forces and Phenomena* (Clarendon Press, Oxford, 1997).
[50] H. Wang, J. Jing, and P. N. Henriksen, J. Vac. Sci. Technol. A **11**, 1987 (1993).
[51] A. Dauscher, M. O. Boffouè, B. Lenoir, R. Martin-Lopez, and H. Scherrer, Appl. Surf. Sci. **138–139**, 188 (1999).
[52] D. J. Bottomley, M. Iwami, Y. Uehara, and S. Ushioda, J. Vac. Sci. Technol. B **17**, 12 (1999).
[53] T. Inuzuka and R. Ueda, J. Vac. Sci. Technol. **6**, 379 (1968).
[54] M. K. Zayed, M. S. Hegazy, and H. E. Elsayed-Ali, Thin Solid Films **449**, 254 (2004).
[55] G. L. Allen, R. A. Bayless, W. W. Gile, and W. A. Jesser, Thin Solid Films **144**, 297 (1986).
[56] K. K. Nanda, S. N. Sahu, and S. N. Behera, Phys. Rev. A **66**, 013208 (2002).
[57] H. W. Sheng, K. Lu, and E. Ma, Acta Mater. **46**, 5195 (1998).
[58] H. J. Koh, P. Rudolph, N. Schäfer, K. Umetsu, and T. Fukada, Mater. Sci. Eng., B **34**, 199 (1995).
[59] Z. Zhou, W. Wang, and L. Sun, Appl. Phys. A **71**, 261 (2000).
[60] K. Mae, V. V. Moshchalkov, and Y. Bruynseraede, Thin Solid Films **340**, 145 (1999).
[61] V. D. Aleksandrov and S. A. Frolova, Inorg. Mater. **40**, 227 (2004).
[62] J. Kritzer, A. Deaconescu, J. de la Parra, Jr., D. F. Coluccio, S. Mikhail, K. Demuren, and R. Q. Topper, Internet J. Chem. **3**, 12 (2000).
[63] V. I. Merkulov and J. S. Lannin, Phys. Rev. B **58**, 7373 (1998).
[64] O. Chamberlian, Phys. Rev. **77**, 305 (1950).